UCID-20261

A NEW "BALANCED" MODE OF OPERATION FOR TMX-U

W. E. Nexsen

January 30, 1985

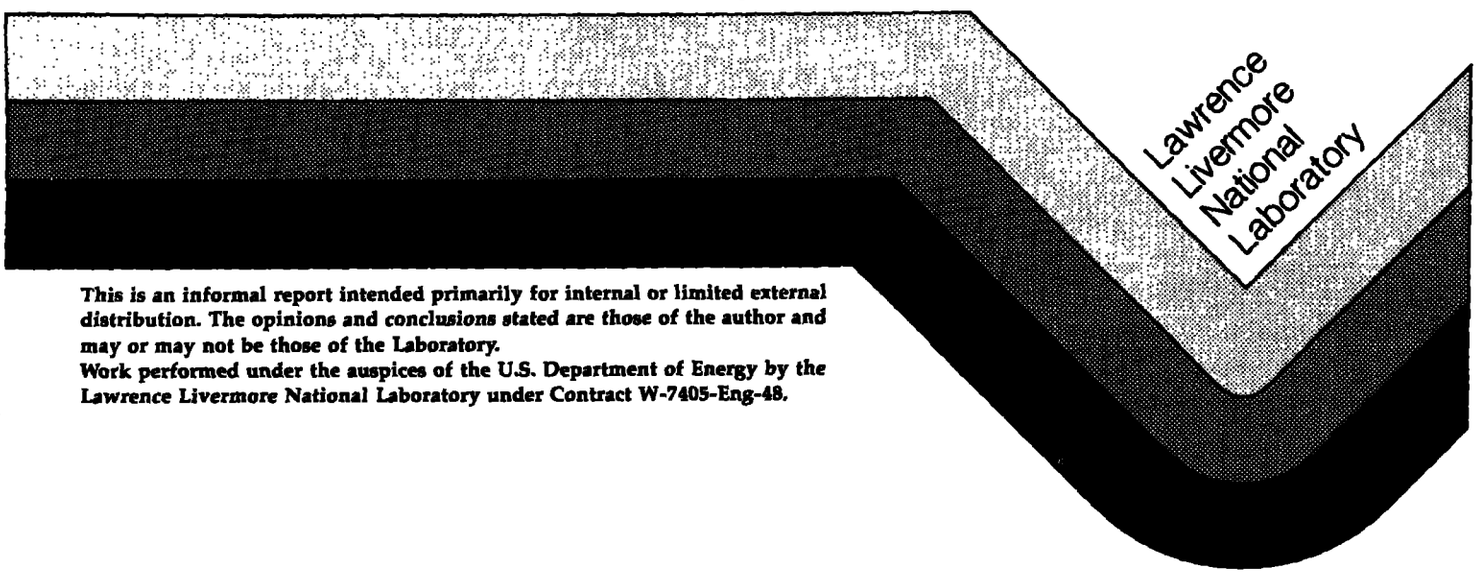

Work performed under the auspices of the U.S. Department of Energy by the Lawrence Livermore National Laboratory under Contract W-7405-Eng-48.

DISCLAIMER

Printed in the United States of America
Available from
National Technical Information Service
U.S. Department of Commerce
5285 Port Royal Road
Springfield, VA 22161
Price: Printed Copy $; Microfiche $4.50

Page Range	Domestic Price	Page Range	Domestic Price
001-025	$ 7.00	326-350	$ 26.50
026-050	8.50	351-375	28.00
051-075	10.00	376-400	29.50
076-100	11.50	401-426	31.00
101-125	13.00	427-450	32.50
126-150	14.50	451-475	34.00
151-175	16.00	476-500	35.50
176-200	17.50	501-525	37.00
201-225	19.00	526-550	38.50
226-250	20.50	551-575	40.00
251-275	22.00	576-600	41.50
276-300	23.50	601-up[1]	
301-325	25.00		

[1]Add 1.50 for each additional 25 page increment, or portion thereof from 601 pages up.

A NEW "BALANCED" MODE OF OPERATION FOR TMX-U

W. E. Nexsen
Lawrence Livermore National Laboratory, University of California
Livermore, CA 94550

ABSTRACT

Under certain, easily reproduced conditions during the January, 1984, period of Tandem Mirror Experiment-Upgrade (TMX-U) operation, relatively dense ($\sim 2 \times 10^{12}$ central cell density), well confined plasmas ($\phi_c/T_c \approx 1.7\text{-}2.7$) have been produced. Under these conditions, the central cell potential appeared to be near ground. We present a scenario to explain this plugging and the axial profile. Simple experimental tests in the future should show whether or not the implied potential profile is correct.

1. INTRODUCTION

In January, 1984, we operated TMX-U for approximately three dozen shots over a period of several days in a manner different from its normal mode. For these shots, we turned off the electron-cyclotron resonant heating (ECRH) at ω_{ce} and $2\omega_{ce}$ before we turned off the sloshing beams. Under these conditions, we commonly observed that the central cell density more than doubled shortly after the ECRH turn off, whereas the end losses dropped by only $\sim$30%. These results imply an improvement in the axial particle confinement. Generally, in the final state

$$n_{plug} < n_c \leq 2n_p$$

and

$$n_c \sim 2 \times 10^{12} \quad .$$

The study of this behavior is the subject of this report.

We have organized this report in the following manner. In Sec. 2, we outline our approach to the data analysis; test the method against some conventional data, where plugging is lost while ECRH is still on; and then present the reduction of one data shot from the January, 1984, series of shots. In Sec. 3, we present a scenario for explaining the observed behavior during these shots and address some of the questions raised about the plausibility of this scenario. In Sec. 4, we discuss the significance of our data. The appendices include the following:

A. Corrections to end-loss analyzer (ELA) data.
B. Details of the data analysis.
C. Scaling toward proposal values.

2. DATA ANALYSIS

The data used for this analysis consists of measurements of both the central-cell line density and the integrated end-loss current from the plasma core. These measurements are combined to give particle axial-containment time for the experiment. In addition, the end-loss analyzer values of ϕ_{EL}, the minimum energy of the end-loss ions; and the spread in energy of the end-loss ions W_{EL} are also used in this analysis. (Corrections to this data for the channel bandwidth are discussed in Appendix A).

The experimental axial confinement time is set equal to the theoretical expression for the axial confinement time using the measured values of density and W_{EL}. Solution of this equation gives an inferred value for the ion confining potential-difference between the plug peak and the central cell. Subtracting this value from ϕ_{EL} gives a value for the central cell potential with respect to ground.

In a similar fashion, assuming low losses of hot electrons and zero nonambipolar radial transport, we set the axial ion losses equal to the axial electron losses to derive a value for the electron confining potential difference. At present, we assume a central-cell electron temperature of $T_e \approx 0.03$ keV. This portion of the calculation is only meaningful when ECRH driven electron losses are not present, i.e., for the present runs when the

ECRH is off. Details of the equations used and the techniques for solution of the equations are given in Appendix B.

As a test of our technique, we first apply it to a conventional shot with the ECRH turned on for most of the shot. Data from such a shot is shown in Figs. 1 and 2. Operating conditions for this shot were very similar to some of the shots in our data set except that part of the ECRH was on for the entire shot. For no readily apparent reason, the end loss current increases in the east end before 50 ms and by 60 ms, neither end appears to be plugged. Figure 2 shows the end-loss analyzer data on axis in the east end after loss of plugging. (These data are corrected for the channel bandwidth as described in Appendix A).

Application of the methods of Appendix B to this data for t = 60 ms, after plugging has been lost out both ends, leads to an implied value of $\phi_c/T_i << 1$, which is outside the range of applicability for the expression $f(\phi/T,R)$. Using a graphic extrapolation of $f(\phi/T,R)$ into this range (see Appendix B for definitions), we estimate roughly that $\phi_c/T_i \approx 0.1$ and $T_i \approx 70$ eV. Thus, this method confirms that the central cell plasma is essentially mirror confined at present.

The end loss potential is virtually the same as the central cell potential under these conditions. The central cell adjusts to equalize ion and electron losses. A reasonable estimate of central-cell electron temperature is in the range of 30 to 50 eV. For these values the central cell potential necessary to equalize collisional losses lies in the range of 100 to 200 V. At 60 ms the measured end loss potential is $\sim$400 V, indicating that the majority of the electron losses must be ECRH driven.

Having confirmed that our method of analysis gives the result expected in the above test case, we now apply it to a member of our data set. Figures 3 and 4 present the data for this shot. The ECRH is turned off at $\sim$44 ms at which time the hot-electron diamagnetism begins to slowly decay. After this time, the only energy inputs are from the neutral beams [the log book records that a "small" amount of ion-cyclotron resonant heating (ICRH) was on]. The central cell density begins to rise when ECRH is turned off and the end losses are reduced at the same time. Density ratios $n_c > n_p$ are obtained late in time; and reduced end losses persist as long as the sloshing beams are turned on.

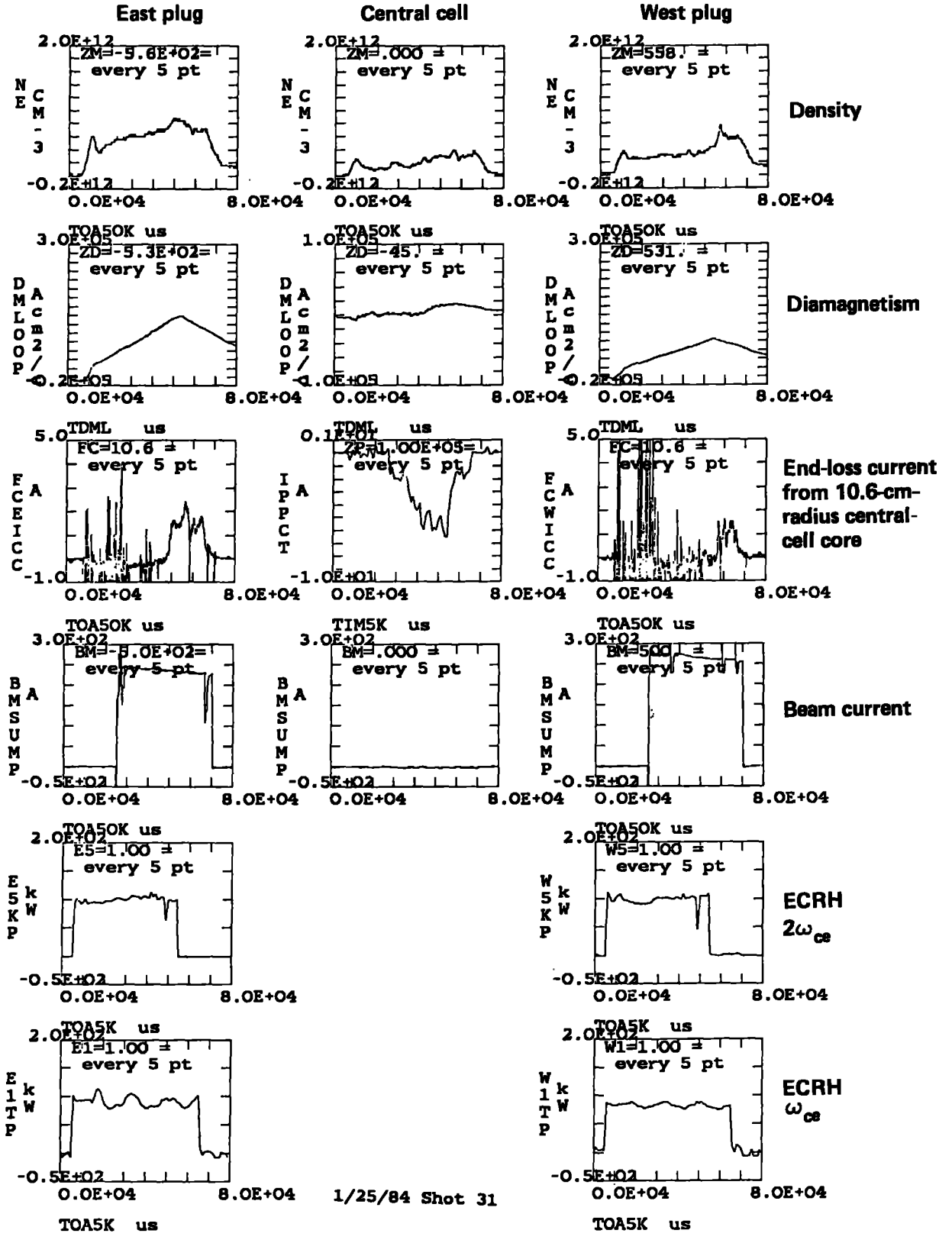

Figure 1. Conventional positive-mode operation.

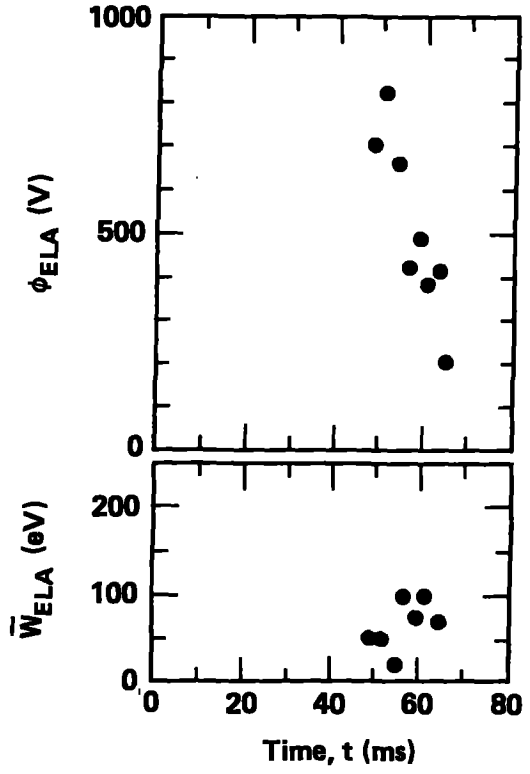

Figure 2. Conventional positive-mode operation end-loss potential and energy. End-loss analyzer data were taken on axis in the east end after loss of plugging.

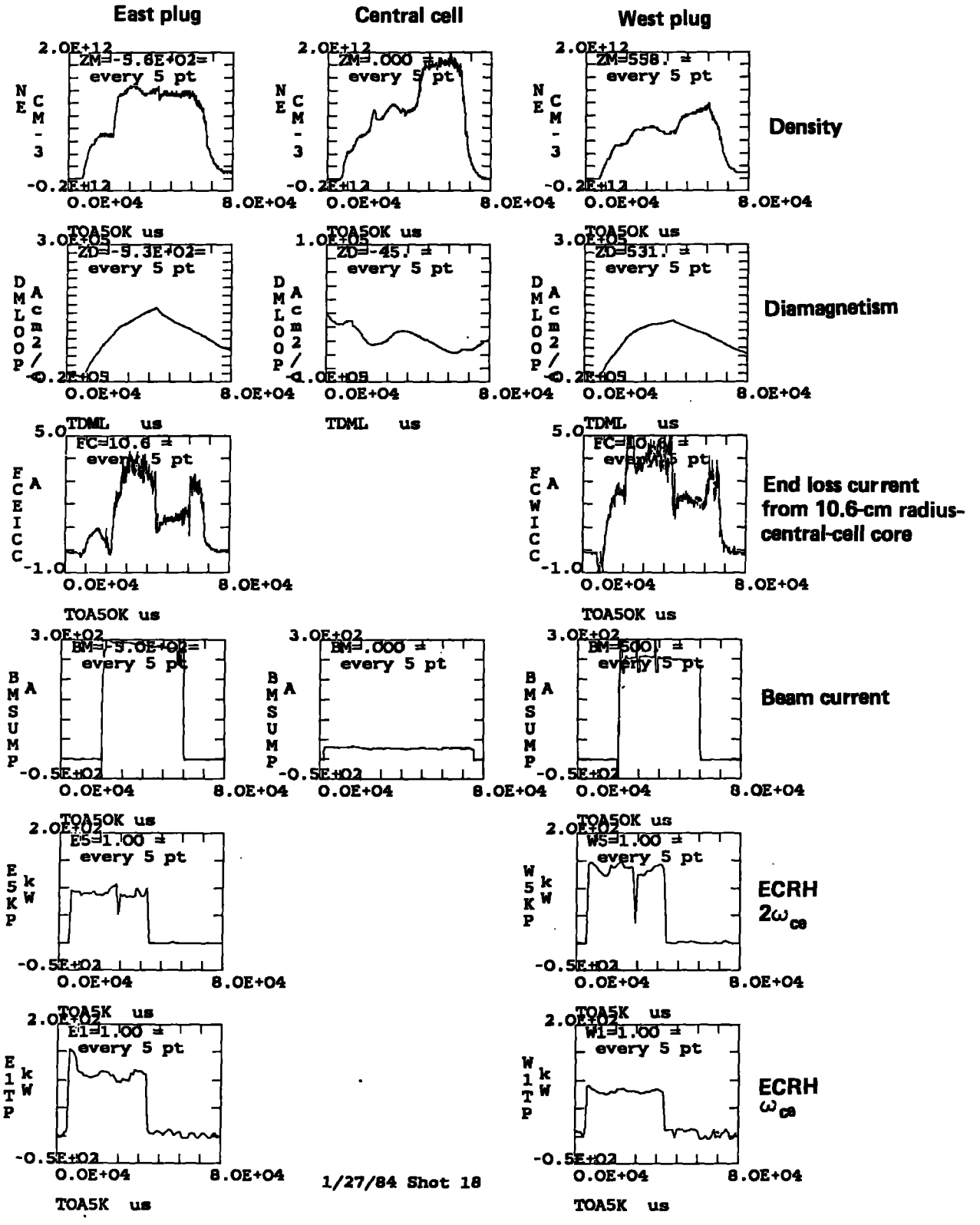

Figure 3. Balanced-mode operation.

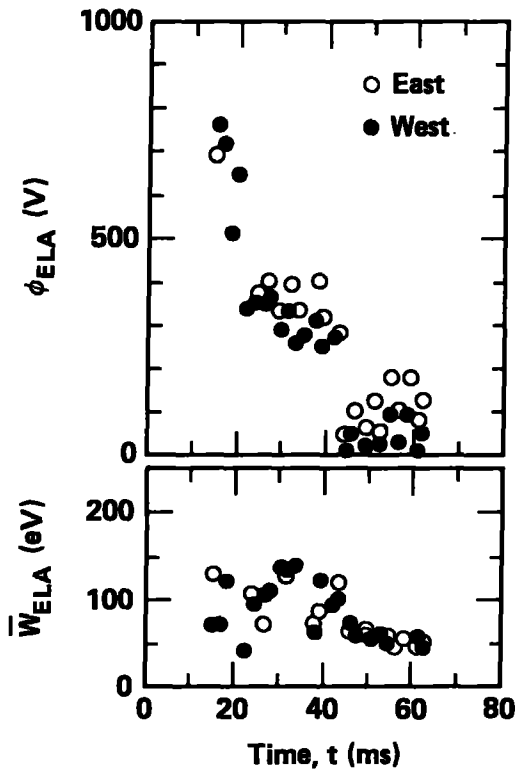

Figure 4. Balanced-mode operation end-loss potential and energy.

Figure 4 shows the variation of ϕ_{EL} and W_{ELA} with time. Note the rapid drop of ϕ_{ELA} at both ends when the ECRH is turned off, the change takes place in less than 2 ms. The reduction of the end-loss energy after the ECRH is turned off may be indicative of the loss of a plasma-potential-driven heating source. (This data has been corrected for the channel bandwidth, see Appendix A).

The results of the analysis for this shot are shown in Fig. 5, which gives the implied axial potential distribution at three different times. Figure 5(a) shows the distribution at 40 ms when the ECRH is still turned on. The end losses at this time are consistent with $\phi_c \approx T_i \approx 0.07$ keV and a central cell potential of ~230 V. Figure 5(b), at 50 ms with ECRH turned off, shows $\phi_c/T_i \approx 2.4$ with $T_i \approx 0.04$ keV, and $\phi_e/T_e \approx 6.9$ (for $T_e = 0.03$ keV is assumed). The central cell potential is at approximately -25 V with respect to ground; whereas the barrier minimum is approximately -240 V below ground and $\phi_{EL} \approx 75$ V above ground. The central cell density rises to almost twice the plug density in this case. Figure 5(c) shows the distribution 10 ms later (shortly before the beam is turned off). At this time, $\phi_c/T_i \approx 2.7$, $T_i \approx 0.032$ keV, $\phi_{EL} \approx 100$ V, and the central cell potential now rises slightly above ground; however, the barrier minimum still remains well below ground.

3. SCENARIO

The following scenario is presented to explain the formation of the potential profiles implied by the data:

- The pumping by the sloshing beams creates a potential dip ϕ_B in the barrier region.
- The ECRH drives electron losses, which causes the central cell potential ϕ_e to rise well above the value expected for simple electron collisional losses.
- Turning off the ECRH eliminates part of the electron losses; and the central cell potential drops to maintain equal ion and electron losses.

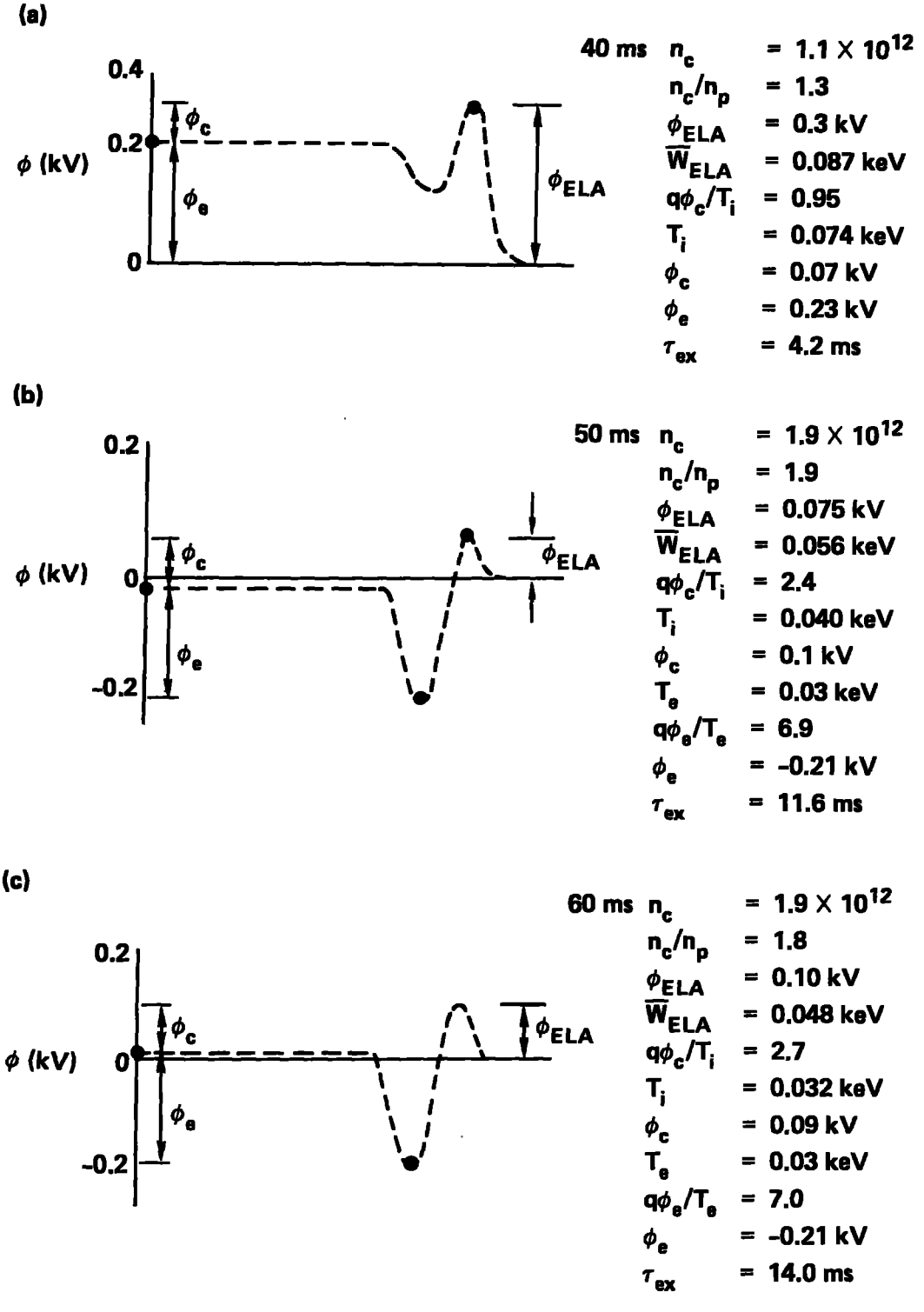

Figure 5. Implied axial potential distribution.

- The barrier minimum dips below ground. Now $\phi_e = \phi_B \approx$ constant, and the maximum electron losses are obtained. If this is still not sufficient to balance the ion losses, the ion confining potential must readjust to reduce the ion losses. In the absence of the sloshing ions (but with the barrier pumped by pump beams or drift pumping), the central cell potential drops well below ground to confine the ions (negative mode of operation).
- When the barrier dips below ground, the electrostatically trapped electrons in the outer sloshing ion turning point region are isolated from the central cell electrons. These electrons, which are fueled by collisional trapping of end-fan electrons and by ionization of cold gas, and are heated by collisions with sloshing ions and hot electrons, develop a positive potential peak to satisfy particle and power balance.
- The end losses equalize with the central cell potential near ground because of the above positive peak.

This scenario fits our observations, but we have some questions about the reasonableness of some of our assumptions concerning the barrier and the positive potential peak.

3.1 IS THE IMPLIED BARRIER DEPTH CONSISTENT WITH AVAILABLE PUMPING?

Pumping

The needed pumping frequency is[1]

$$\nu = \frac{n_{pass}}{n\tau_p} \left[0.935\ (1 + 0.0441R)\ \frac{g}{g-1}\right]^{1/0.3} H \times (g - 1) \quad ,$$

where

$$n\tau_p = 3 \times 10^{10} \left[T_i\ (keV)\right]^{3/2} \quad ,$$

$$n_{pass} = \frac{n_c}{R(1 + \pi_e \phi_e / T_i)^{1/2}} \quad ,$$

$$R = B_{IM}/B_b \approx 4.7 \quad ,$$

$$g = \frac{n_{trap} + n_{pass}}{n_{pass}} \quad ,$$

and H is a shape factor.

We take the conditions at 60 ms for our test shot (1/27/84/18). Taking

$$T_i = 0.032 \text{ keV},$$

$$|\phi_e| = 0.21 \text{ keV},$$

$$n_c = 1.9 \times 10^{12},$$

$$n_e(b) = 10^{12},$$

$$n_{SL}(b) \approx 4 \times 10^{11} \text{ (from SED calibration)} \quad ;$$

we find

$$n_{pass} = \frac{1.9 \times 10^{12}}{4.7\left(\pi \frac{0.21}{0.032} + 1\right)^{1/2}} \approx 0.9 \times 10^{11} \quad ,$$

$$g = \frac{10^{12} - 4 \times 10^{11}}{0.9 \times 10^{11}} \approx 7 \quad ,$$

$$n\tau_p = 3 \times 10^{10} (0.032)^{3/2} \approx 1.7 \times 10^{8} \quad ,$$

and

$$\nu \approx 1.3 \times 10^{3} \text{ H} \times 6 = 7.8 \times 10^{3} \text{ H} \quad .$$

The available beam pumping by charge exchange at the plug center plane is

$$\nu_{cx} = \hat{n}_b \langle\sigma v\rangle_{cx} \quad ,$$

where $\hat{n}_b$ is the peak beam density. Using the values[2]

$$\hat{n}_b = 10^8 \, I_{accel} \quad ,$$

for an accel-current of 280 A and with $\langle\sigma v\rangle_{cx} = 10^{-7}$, we find

$$\nu_{cx} \simeq 2.8 \times 10^3 \quad .$$

Thus it appears that only about one-third of the pumping required by theory is available. Because the theory has not been tested experimentally, and, indeed, discrepancies have been noted during standard positive mode operations, we do not feel that this disagreement is enough to negate our analysis of the balanced mode.

3.2 IS THE MEASURED POSITIVE POTENTIAL PEAK CONSISTENT WITH OUR BEST ESTIMATES OF PARTICLE AND POWER BALANCE IN THAT REGION?

The group of electrostatically trapped electrons in the positive potential peak are isolated from the central cell electrons by the negative barrier, and are heated by drag on the sloshing ions and mirror confined hot electrons. We assume these electrons are in contact with a passing group of cold electrons, which are confined between the wall and the negative potential dip and are clamped at a temperature T_u. In the region between the wall and the peak of the outer mirror, the cold electron density satisfies

$$n_{eu}(z) = n_{iEL}(z) + n_{iu} \quad .$$

Where n_{iEL} is the ion end-loss density, and n_{iu} is the isotropic cold-end-fan plasma density. We assume that n_{eEL} is much less than n_{ev}. From measurements on TMX,[3] we estimate that T_u is about 5 eV and that n_{iu} is about 2×10^9 cm^{-3} at the wall.

We apply the theory of particle and energy exchange between untrapped and electrostatically confined populations in magnetic mirrors[4] to calculate the temperature T_t of the trapped population and n_m the value of n_{eu} at the outer mirror throat, which are consistent with the observed potential. Following Ref. 4, we first ignore the trapped particle source current to solve the rate equations, returning later to justify this simplification. In this approximation steady-state particle balance gives

$$\phi/T_t = -\ln\left[\frac{n_m}{n_t}\left(\frac{T_t}{T_v}\right)^{1/2}\right] \quad , \tag{1}$$

and

$$\left(1 + \frac{\hat{\tau}_p}{\tau_v}\right)(T_t - T_u) \approx \frac{\tau_p}{n_t} P \quad , \tag{2}$$

where

$$\tau_p = \tau_{ee} f_e\,(\phi/T_t, R) \quad , \tag{3}$$

$$\hat{\tau}_p = \tau_p \exp(-\phi/T_t) \quad , \tag{4}$$

$$1/\tau_v = \frac{2}{\pi^{1/2}\tau_{ee}R} \times \frac{T_t}{\phi} \quad . \tag{5}$$

and P is the input power density.

We use the axial distribution of Fig. 6 for the various particle groups to calculate the power input from drag. The justification of the distributions is explained in the following topics.

Hot Electrons

We assume that the hot-electron distribution is flat to z ≃ 580 cm after which the drop-off is fitted with a Gaussian to match the diamagnetic loop ratios. The density ratios implied by the loop ratios for hot electrons alone are indicated by the crosses in Fig. 6.

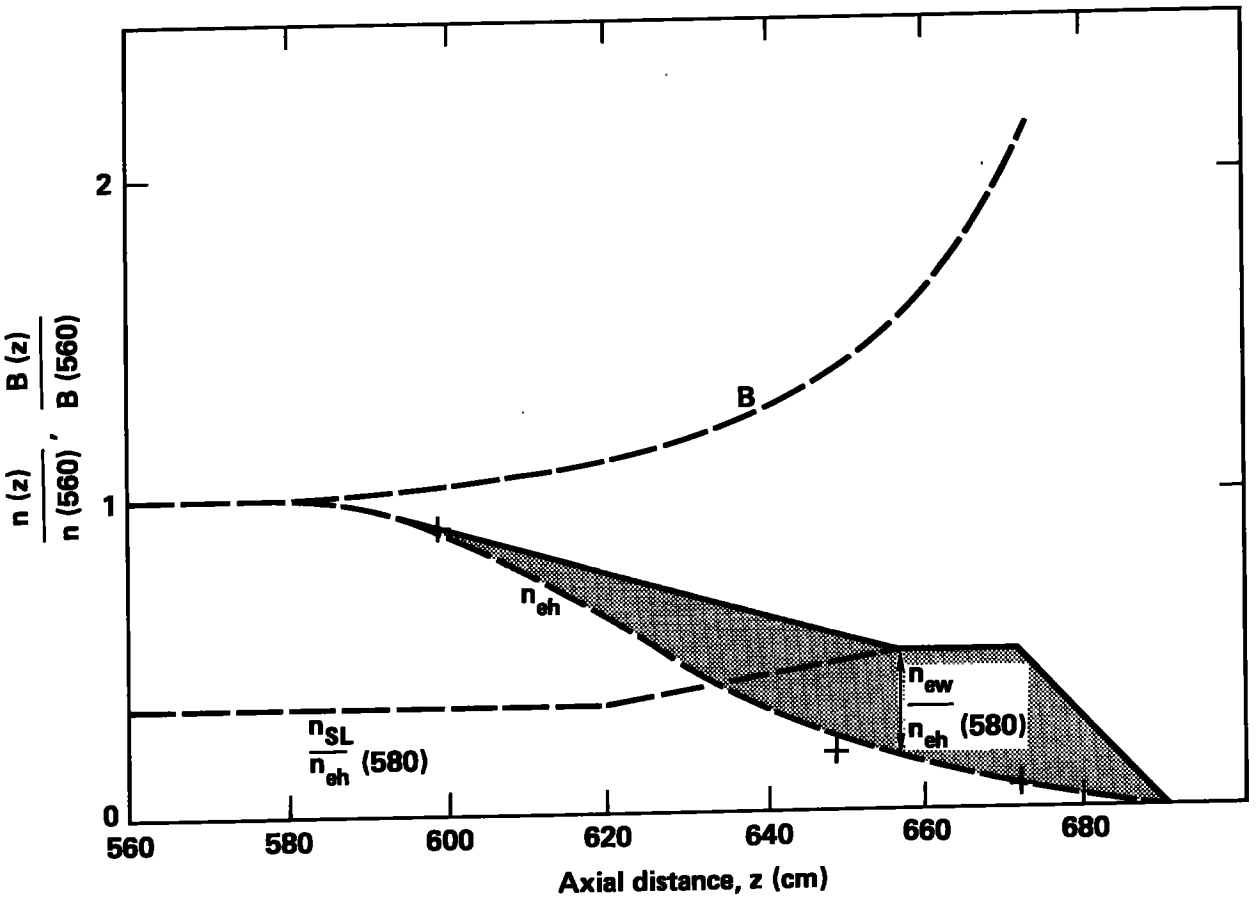

$$B_0 \int_{580}^{690} \frac{dz}{B} = 82 \text{ cm}$$

$$B_0 \int \frac{n_{ew}\, dz}{B} = 13.5 \left[n_{eh}\,(580)\right]$$

$$B_0 \int \frac{n_{eh}}{B} dz = 50 \left[n_{eh}\,(580)\right]$$

$$B_0 \int \frac{n_{ew}^2}{B} dz = 3.8 \left[n_{eh}\,(580)\right]^2$$

$$B_0 \int \frac{n_{eh}\, n_{ew}}{B} dz = 4.1 \left[n_{eh}\,(580)\right]^2$$

$$B_0 \int \frac{n_{SL}\, n_{ew}}{B} dz = 5.8 \left[(n_{eL}\,(580)\right]^2$$

Figure 6. Axial distribution for various particle groups.

Sloshing Ions

For sloshing ions, the secondary emission detector (SED) calibration yields a value of $n_{si}(657)/n_{total}(568) \approx 0.7$ if we assume flux mapping. Modeling of finite Larmor radius (FLR) effects in the fan,[5] which result in longer line lengths through the minor diameter, led us to reduce the density to 0.5. Near the center plane, where FLR effects are not as important, we take

$$n_{si}(568)/n_{total}(568) \approx 1/2 \left.\frac{n_{si}(657)}{n_{tot}(568)}\right|_{FLR=0} = 0.35.$$

The sloshing ion distribution is assumed to extend to the z = 673 cm region because the presence of sloshing ions usually doubles the loop signal at this point over the value with hot electrons alone. Because the hot electron energy is ≈10 times the sloshing ion energy, we assume that the sloshing ion density is ≈10 times the hot electron density under this loop. The linear sections of the distribution more or less match the shape predicted by Fokker-Planck runs.

Total Electron Density

A straight line connection is made from the tangent to hot electron distribution at z ≈ 590 cm, where $n_e = n_{eh}$ to z ≈ 657 cm, where $n_e = n_{et} + n_{eh} = n_{SI}$.

The bounce averaged power input in keV/cm^2 is given by

$$PL = \left(\frac{\bar{E}_{si}}{10^9\ T_e^{3/2}}\ B_0 \int_{580}^{690} \frac{n_{si}\ n_{ew}}{B}\ dz + \frac{B_0}{2.7 \times 10^5}\ \bar{E}_h^{1/2} \int \frac{n_{he}\ n_{ew}}{B}\ dz \right) \times 10^{-3} \quad ,$$

where energy units are in keV.

For the assumed axial distribution and E_{si} = 6 keV, E_h = 70 keV

$$PL = \left(\frac{3.5 \times 10^{-11}}{T_t^{3/2}} + 1.81 \times 10^{-9} \right) n_{eh0}^2 \quad ,$$

where $n_{eh0} = n_{eh}(580)$. Taking

$$\frac{\tau_p}{n_t} P = \frac{n\tau_p}{n_t^2 L} PL \quad ,$$

$$n\tau_p = 4.35 \times 10^8 \, T_t^{3/2} \, f_e(\phi/T,R) \text{ (see Appendix B)} \quad ,$$

and

$$n_t^2 L = 3.82 \, n_{eh0}^2 \quad ;$$

we obtain

$$\frac{\tau_p P}{n_t} = [4 \times 10^{-3} + 0.2 \, T_t^{3/2}] \, f_e(\phi/T,R) \quad . \tag{6}$$

Substituting Eqs. (3), (4), (5), and (6) in Eq. (2) and rearranging, we obtain

$$T_t = (4 \times 10^{-3} + 0.2 \, T_t^{3/2}) \, \frac{(\phi/T_t) \exp(\phi/T_t)}{[(\phi/T) \, k_e(\phi/T,R) + \frac{2}{\sqrt{\pi}} R} + T_u \quad , \tag{7}$$

where

$$k_e(\phi/T,R) = \frac{\exp(\phi/T)}{f_e(\phi/T,R)} \quad .$$

For $R = 2$, $\phi = 0.1$ and $T_u \approx 0.006$, we find a solution of Eq. (7) for $T_t \simeq 0.056$ keV. Using $\phi/T_t = 0.1/0.057 = 1.75$ and $T_t/T_u \approx 10$, Eq. (1) gives

$$\frac{n_m}{n_t} \simeq \left(\frac{T_u}{T_t}\right)^{1/2} \exp(-1.75) = 0.055 \quad .$$

For

$$n_t = 4 \times 10^{11} \quad ,$$

it follows that

$$n_m = 2 \times 10^{10} \quad .$$

We compare this value of n_m with that expected for the density of the central-cell end losses in the mirror throat,

$$1/2\ nqvA = I_{EL}$$

where we assume there is no ion flow back towards the central cell at the peak of the outer mirror. Solving for n

$$n = \frac{2\ I_{EL}(10.6)}{q \times 10^6 \times \frac{B_0}{B_m} \times \pi(10.6)^2\ (\overline{W}_{EL} + \phi_{EL})^{1/2}} \quad .$$

For $I_{EL}(10.6) = 1.5$ A, $\phi_{EL} + W_{EL} = 150$ eV, $B_0/B_m = 0.15$

$$n \approx 3 \times 10^{10} \quad .$$

Considering the crudeness of the model the agreement is good.

The validity of ignoring the source term in our solution is based on the following condition:[4]

$$S \frac{\hat{\tau}_p}{n_t} << \left(\frac{T_c}{T_u}\right)^{1/2} \frac{n_m}{n_{t\ max}} \quad ,$$

where S is the trapped-particle source current and $\hat{\tau}_p = \tau_p \exp(-\phi/T)$.

We set

$$\frac{S\ \hat{\tau}_p}{n_t} = \frac{\int \frac{Sdz}{B}}{\int \frac{n_t}{\tau_p} \frac{dz}{B}} = \frac{\int \frac{Sdz}{B}}{\int \frac{n_t^2\ dz}{B}} \times (n\hat{\tau}_p) \quad ,$$

where

$$\int \frac{Sdz}{B} = \left(\langle\sigma v\rangle_{ihe} \int \frac{n_{en} n_0}{B}\ dz + \langle\sigma v\rangle_{Lwe} \int \frac{n_{ew} n_0 dz}{B} + \langle\sigma v\rangle_{iSi} \int \frac{n_{si} n_0 dz}{B}\right) \quad .$$

Sloshing ion densities are consistent with a charge exchange lifetime of ~2 ms or a bounce averaged neutral density of

$$\langle n_0 \rangle \simeq \frac{1}{\tau_{cx} \langle \sigma v \rangle_{cx}} = 5 \times 10^9 \quad ,$$

for $\langle \sigma v \rangle_{cx} = 10^{-7}$. The TMX-U data shows that the ratio of sloshing ion density to total density is rather insensitive to total density. This is consistent with most of the charge exchange losses taking place in the thin fan regions where increasing the density gives little shielding improvement. We model the neutral density by the following:

$$n_0 = 0 \qquad 568 < z < 620 \quad ,$$

$$n_0 = 10^{10} \qquad 620 < z \quad ,$$

(assuming a similar distribution on the inboard side of the plug center plane and that the ions spend half their bounce time in the fans). Using the model and setting $\langle \sigma v \rangle_{ihe} = 6 \times 10^{-9}$, $\langle \sigma v \rangle_{iwe} = 4 \times 10^{-8}$, $\langle \sigma v \rangle_{isi} = 4 \times 10^{-9}$, we obtain

$$B_0 \int \frac{S dz}{B} = 7 \times 10^3 \, n_{ehO} \quad ,$$

and with

$$B_0 \int \frac{n_t^2 dz}{B} = 3.8 \, n_{ehO}^2 \quad ,$$

$$n\hat{\tau}_p = 4.35 \times 10^8 \, T_t^{3/2} \, f_e(\phi/T, R) \exp(-\phi/T) \quad ;$$

and setting

$$T_e = 0.057, \; n_{ehO} = 10^{12} \quad ,$$

and

$$f_e(1.75,2)\ \exp(-1.75) = 2.2 \quad ;$$

we obtain

$$\frac{S\hat{\tau}_p}{n_t} \approx 0.024 << \left(\frac{T_t}{T_v}\right)^{1/2} \frac{n_m}{n_{t\,max}} = (10)^{1/2}\ \frac{2 \times 10^{10}}{4 \times 10^{11}} = 0.16 \quad .$$

Thus, our approximation was justified.

4. DISCUSSION

The mode of operation described here is different enough from either the positive or negative mode of operation to warrant a new name, the "balanced" mode. In the positive (negative) mode, central cell ions (electrons) are contained by potential peaks (minimums) in the end cells while the central cell potential adjusts with respect to the end walls to maintain equal ion and electron losses. The presence of a potential double layer in the balanced mode allows the central cell to ride near ground potential while maintaining equal end losses.

For stable balanced mode operation, the positive potential peak must be referenced to the external ground so that heating the electrons electrostatically confined in the potential peak drives them into the loss cone. Thus we may wish to avoid the strong rf limit of heating, which generally moves the electrons into the mirror trapped groups and causes the potential to be referenced to the barrier minimum. Because the barrier minimum is in turn referenced to the central cell potential, any excess of central-cell electron losses over ion losses (as may arise from ECRH heating) will probably produce a rapid transition back to the positive mode. With isotropic heating of the electrons in the potential peak by drag or by ECRH in the weak limit, the electrons will be lost through the lower potential barrier into the loss cone and to the end walls. In this case, any excess in central cell electron losses results in the central cell potential rising. Since the positive

potential peak is now fixed with respect to ground, the rise in the central cell potential decreases the ion confining potential, allowing the losses to equalize. Thus, a stable balanced mode seems achievable under these conditions.

Since the transient time scale for the balanced mode with no ECRH appears to be on the order of the hot-electron decay time, many milliseconds of operation with good containment appears possible (in fact no loss of plugging has been observed before the sloshing beams are turned off).

The balanced mode, if it can be maintained with ECRH turned on and scaled to higher confining potentials, offers certain important advantages as an operating mode. One of the most important advantages is that operation of the central cell at potentials near the ground potential of the walls greatly reduces the drive for resonant radial transport and rotational instabilities.

The balanced mode also offers a bridge to allow the study of the pure negative mode. By bringing in pumping beams and dropping out sloshing beams, we should be able to make the transition from the balanced mode to the negative mode. The negative mode is attractive because it dispenses with sloshing beams and ECRH heating at the outer 10-kG point. If azimuthal asymmetry of plugging is a problem in the balanced and positive mode, it may be much less of a problem in the negative mode (that is if the azimuthal asymmetry of plugging is due to FLR effects of the sloshing ions). In addition, if secondary electrons are causing problems now, the negative mode should exclude them. Like the positive mode, the negative mode will probably require the use of potential control plates to maintain the central cell potential near ground.

Important questions exist concerning the ability to operate TMX-U in the negative mode because of the possible formation of sheaths in the barrier region. Consequently, we have been hesitant to devote any time or effort to this mode because negative-mode studies would interfere with our studies of the positive mode. However, by simply remounting the pump beams, we should be able to study this mode in the transient case without having to move the ECRH feed.

The verification of the existence of the balanced mode of operation and its exploitation should be an important part of the experimental goals for TMX-U.

REFERENCES

1. A. H. Futch and L. L. LoDestro, Collisional Trapping Rates for Ions in a Magnetic and Potential Well, Lawrence Livermore National Laboratory, Livermore, CA, UCRL-87249 (1982).

2. D. L. Correll, Sloshing-Ion-Rate Equation (TMX-U), Lawrence Livermore National Laboratory, Livermore, CA, Magnetic Fusion Energy Memorandum, MFE/CP/83-4150m/0452m (April 27, 1983).

3. P. Coakley, N. Hershkowitz, and G. D. Porter, "End-Wall Plasma Characteristics in the Tandem Mirror Experiment," Nucl. Fusion 22, 1321 (1982).

4. R. H. Cohen, I. B. Bernstein, J. J. Dorning, and G. Rowlands, "Particle and Energy Exchange Between Untrapped and Electrostatically Confined Populations in Magnetic Mirrors," Nucl. Fusion 20, 1421 (1980).

5. W. E. Nexsen, FLR Modification of Axial Plugging Symmetry, Lawrence Livermore National Laboratory, Livermore, CA, Magnetic Fusion Energy Memorandum 5684r/0486r/WEN/jdb (January 18, 1984).

APPENDIX A: CORRECTIONS TO END-LOSS-ANALYZER DATA

Because of the high plasma potentials present for at least part of most TMX-U shots, we must use high end-loss-analyzer sweep voltages. Consequently, if the ion temperature is low, the voltage sweeps through the end-loss-current cut off so rapidly that the signal should be corrected for the channel bandwidth; otherwise the ion end loss energy is overestimated. The shape of the uncorrected end-loss current vs time is seen in Fig. A-1(a), where the current is rounded on both the rise and fall by the finite bandwidth. If J_1 is the recorded, uncorrected data

$$J_1 = \frac{\exp(-t/\tau)}{\tau} \int_{-\infty}^{t} J_0 \exp(t/\tau)\, dt \quad ,$$

where J_0 is the original undistorted signal. Solving for J_0

$$J_0 = J_1 + \tau \frac{dJ_1}{dt} \quad .$$

Figure A-1(b) shows the data of A-1(a) with this correction applied, using $\tau \approx 54$ μs.

Figure A-2 depicts the corrected data plotted over the uncorrected computer output. As expected, the potential is more or less unchanged, but the corrected end-loss energy is approximately one-half of the uncorrected value. We plan to include this correction in the ELA software, but currently this correction, when necessary, must be performed off line.

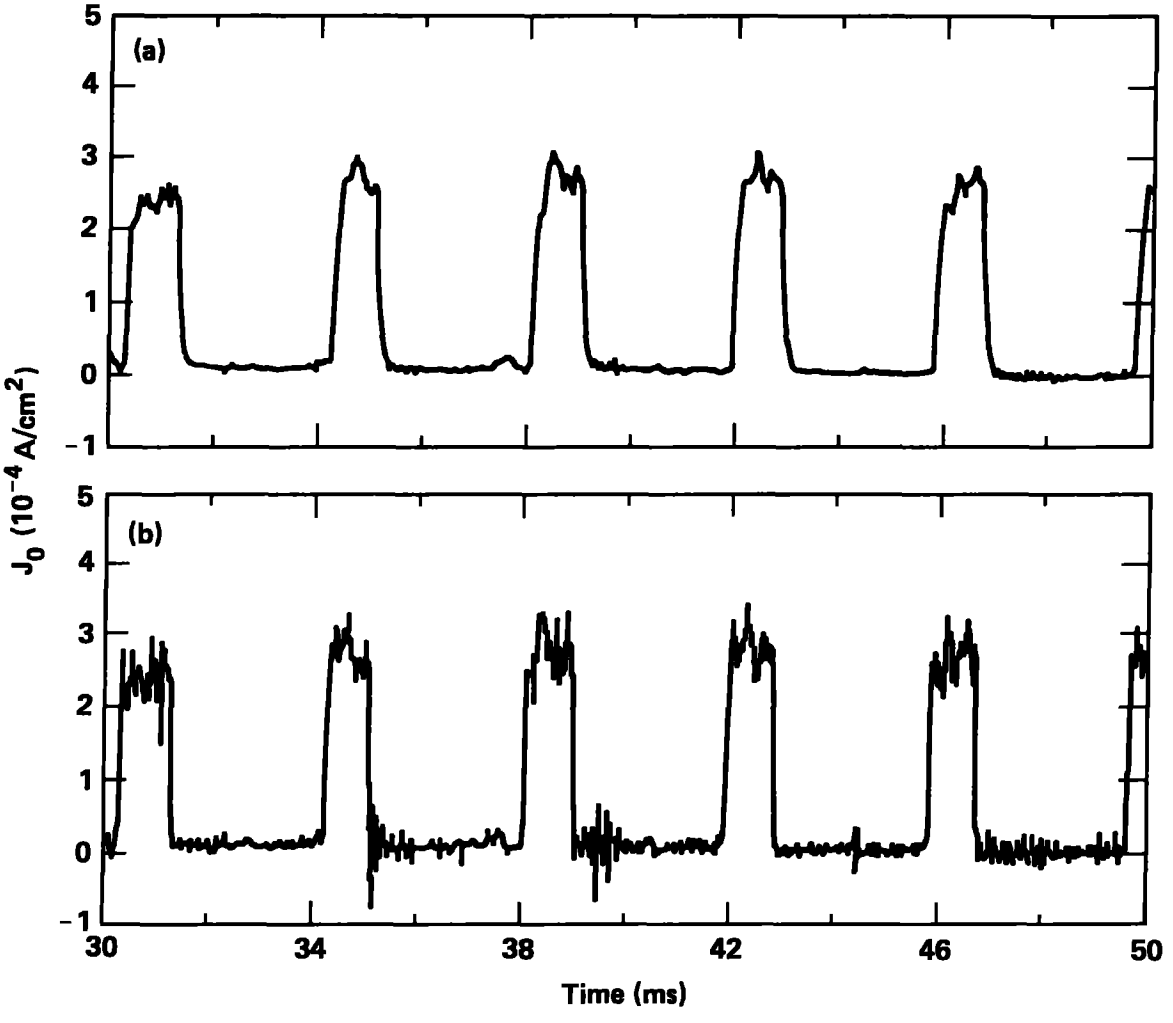

Figure A-1. The shape of the uncorrected end-loss current vs time, where the current is rounded on both the rise and fall by the finite bandwidth.

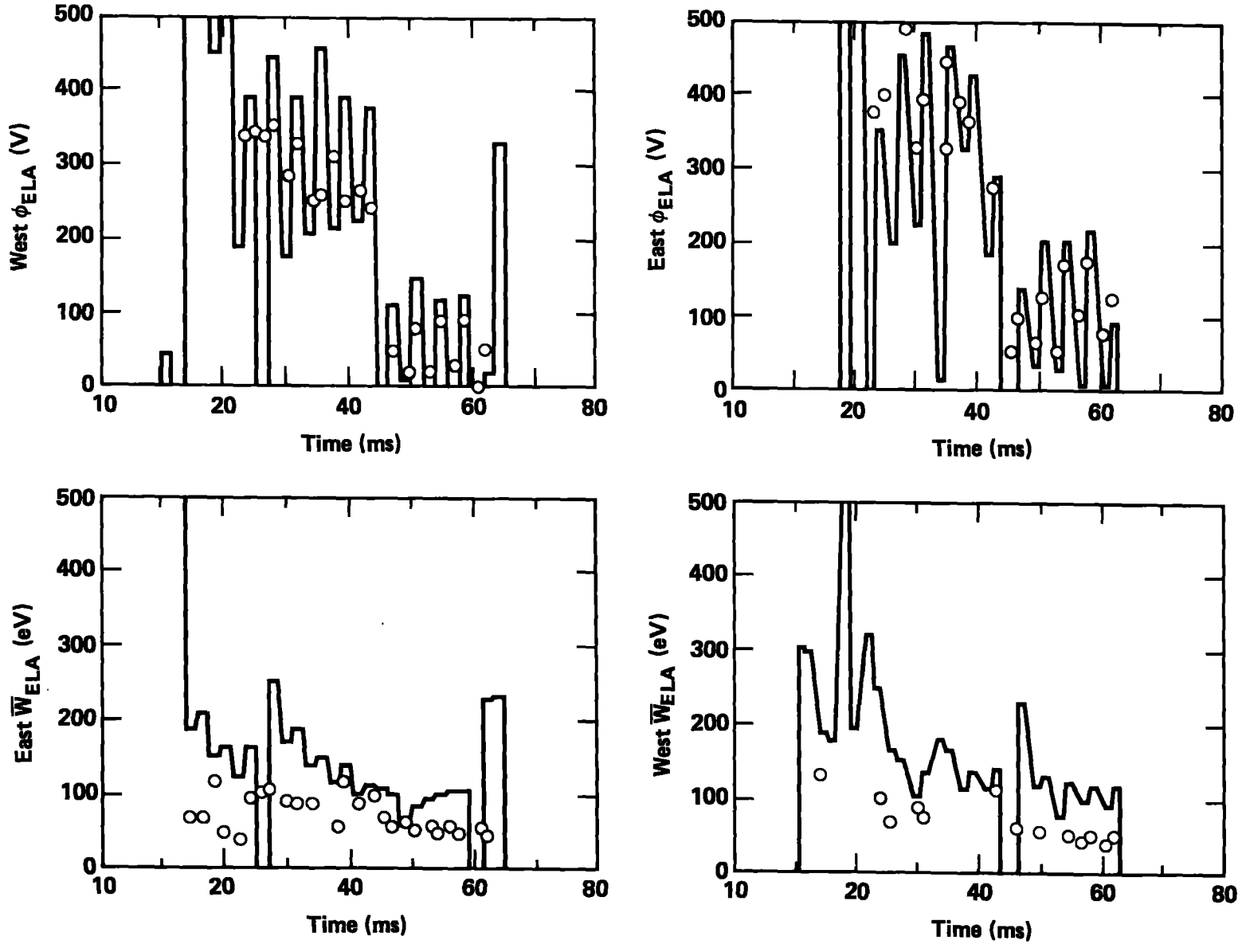

Figure A-2. The corrected end-loss potential and energy vs time data plotted over the uncorrected computer output.

APPENDIX B: DATA ANALYSIS METHOD

Following Rognlien and Cutler (Ref. B-1), we set

$$\tau_{II} = \tau_c + \tau_p \quad ,$$

$$\overline{W}_{EL}/T_i = (2\tau_c + \tau_p)/(\tau_c + \tau_p) \quad ,$$

where

$$\tau_c = \sqrt{\pi}\,\frac{RL}{v_i}\exp(\phi/T)$$

$$= \tau_f \exp(\phi/T) \quad .$$

For R = 8.5/3, L = 510, deuterium ions

$$\tau_f = \frac{0.082 \text{ ms}}{[T(\text{keV})]^{1/2}} \quad , \tag{B-1}$$

and

$$\tau_p = \tau_0 \, f(\phi/T,R) \quad .$$

Here

$$n\tau_0 = \left(\frac{m}{2}\right)^{1/2} \frac{T_i^{3/2}}{\pi e^4 \ln\lambda} = 2.61 \times 10^{10} \left(\frac{A}{2}\right) [T_i(\text{kev})]^{3/2} .$$

For deuterium

$$\tau_0 = \frac{90\,[T_i(\text{keV})]^{3/2}}{\overline{nl}_c^{13}} \text{ ms} \quad , \tag{B-2}$$

where $\overline{nl}_c^{13}$ is the central-cell line density in units of 10^{13}, and we have assumed a parabolic radius of 26 cm.

For $f(\phi/T, R)$, we use the expressions of Najmabadi, Conn, and Cohen (Ref. B-2) to produce the plots of Fig. B-1.

For the 10.6-cm-radius central-cell core

$$\tau_{\parallel ex} = \frac{8.15\ \overline{nT}_c^{13}}{\sum I_{EL}(10.6)}\ \text{ms} \quad , \tag{B-3}$$

where $\sum I_{EL}(10.6)$ is the sum of the radially integrated end-loss currents from the 10.6-cm-radius core (assuming azimuthal symmetry of the end losses). The azimuthal symmetry assumption is commonly used in all of our data analysis. Although both experimental data and theoretical reasons exist that indicate the above is not completely correct, we believe that the corrected values would only change numbers without changing conclusions.

We measure $\overline{nT}_c^{13}$, $\overline{W}_{EL}$, $\sum I_{EL}(10.6)$. For ions we assume $R \approx 8.5/3 \approx 3$ and that

$$\tau_{\parallel ex} = \tau_{\parallel} = \tau_c + \tau_p \quad ,$$

or

$$\frac{\tau_{\parallel ex}}{\tau_0} = f(\phi/t,3)\left[1 + \frac{\tau_f}{\tau_0} K(\phi/T,3)\right] \quad ,$$

where

$$K(\phi/T,3) = \exp(\phi/T)/f(\phi/T,3) \quad ,$$

(see Fig. B-2). From Eqs. (B-2) and (B-3)

$$\frac{\tau_{\parallel ex}}{\tau_0} = \frac{9 \times 10^{-2}\ (\overline{nT}_c^{13})^2}{\sum I_{EL}(10.6)\ [T_c(\text{keV})]^{3/2}} \quad . \tag{B-4}$$

From Eqs. (B-1) and (B-3)

$$\frac{\tau_f}{\tau_0} = \frac{9.1 \times 10^{-4}(\overline{nT}_c^{13})}{[T_c(\text{keV})]^2} \quad . \tag{B-5}$$

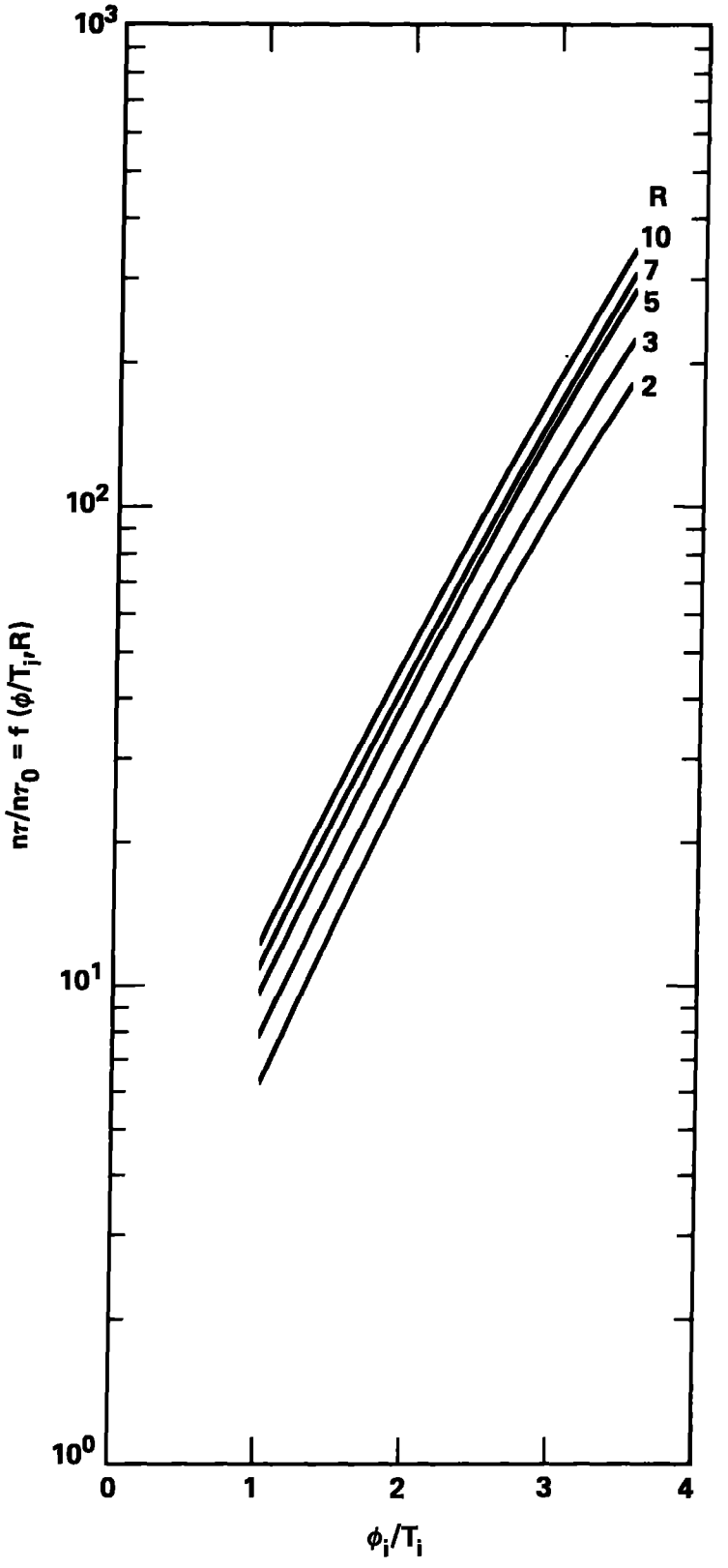

Figure B-1. Plots using the expressions from Ref. B-2. For ions we plot $n\tau_p/n\tau_0 \equiv f(\phi_i/T_i,R)$ versus ϕ_i/T_i with R as a parameter.

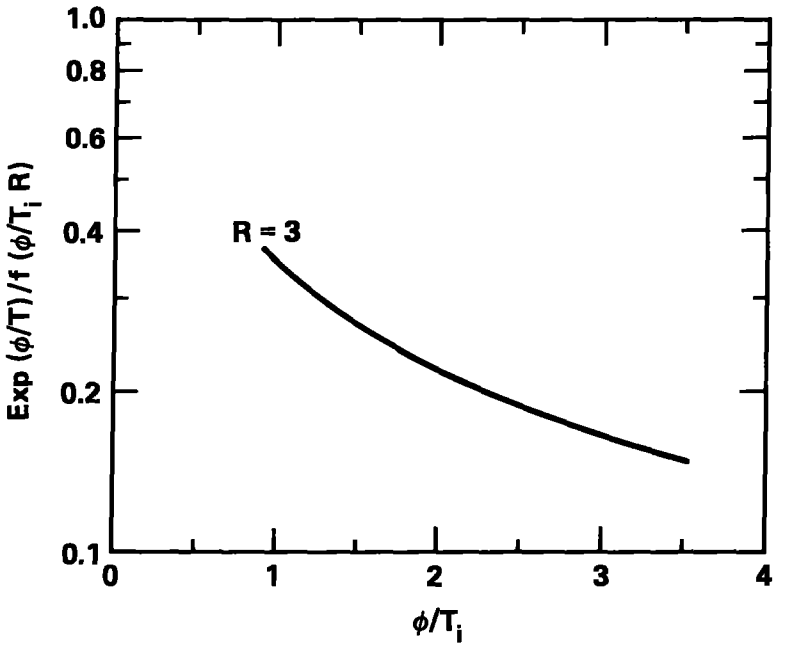

Figure B-2. For ions we plot for R = 3

$$K(\phi_i/T_i,3) \equiv \exp(\phi_i/T_i)/f(\phi_i/T_i,3) \text{ versus } \phi_i/T_i \quad .$$

Also

$$T_i = \bar{W}_{EL}\left[\frac{1 + (\tau_f/\tau_0)\ K(\phi/T,3)}{1 + 2(\tau_f/\tau_0)\ K(\phi/T,3)}\right] \ .$$

For the first iteration assume

$$(T_i)_0 = \bar{W}_{EL} \ ,$$

to calculate $(\tau_{\|ex}/\tau_0)_0$ and $(\tau_f/\tau_0)_0$ from Eqs. (B-4) and (B-5), and solve

$$f(\phi/t,3) = \left(\frac{\tau_{\|ex}}{\tau_0}\right)_0\left[\frac{1}{1 + \left(\frac{\tau_f}{\tau_0}\right)_0 K(\phi/T,3)}\right]$$

for $(\phi/T_i)_0$. For subsequent iterations set

$$(T_i)_{j+1} = \bar{W}_{EL}\left[\frac{1 + (\tau_f/\tau_0)_j\ K((\phi/T)_j,3)}{1 + 2(\tau_f/\tau_0)_j\ K((\phi/T)_j,3)}\right] \ ,$$

to repeat the loop. The process usually converges in about three iterations.

We follow a similar process for the electrons. If there are no nonambipolar electron losses, we require

$$(\tau_{\|ex})_{ions} = (\tau_{\|ex})_{electrons} = \tau_{\|ex} \ ,$$

and set

$$\tau_{\|ex} = (\tau_c + \tau_p)_e$$

$$= \tau_{fe}\ \exp(\phi_e/T_e) + \tau_{ee}\ f_e(\phi_e/T_e,R) \ ;$$

where for R = 5/3, L = 510

$$\tau_{fe} = \frac{\sqrt{\pi}\ RL}{v_e} = \frac{8.0 \times 10^{-4}}{[T_e(keV)]^{1/2}} \ ms \ ,$$

$$n\tau_{ee} = 4.35 \times 10^{8} \, [T_e(\text{keV})]^{3/2} \quad ,$$

or

$$\tau_{ee} = \frac{1.5 \, [T_e(\text{keV})]^{3/2}}{\overline{nT}_c^{13}} \ \text{ms} \quad .$$

Then

$$\left(\frac{\tau_{\parallel ex}}{\tau_{ee}}\right) = \frac{5.43 \, (\overline{nT}^{13})^2}{\sum I_{EL}(10.6) \, [T_e(\text{keV})]^{3/2}} \quad ,$$

$$\left(\frac{\tau_f}{\tau_{ee}}\right) = \frac{5.3 \times 10^{-4} \, (nl^{13})}{[T(\text{keV})]^2} \quad .$$

Figure B-3 shows $f_e(\phi_e/T_e, 1.67)$, whereas Fig. B-4 shows $K_e(\phi_e/T_e, 1.67)$. Assuming $T_e = 0.03$, we solve

$$f_e(\phi_e/T_e, 1.67) = \left(\frac{\tau_{\parallel ex}}{\tau_{ee}}\right)\left[\frac{1}{1 + (\tau_f/\tau_{ee}) \, k_e(\phi_e/T_e, 1.67)}\right]$$

for ϕ_e/T_e.

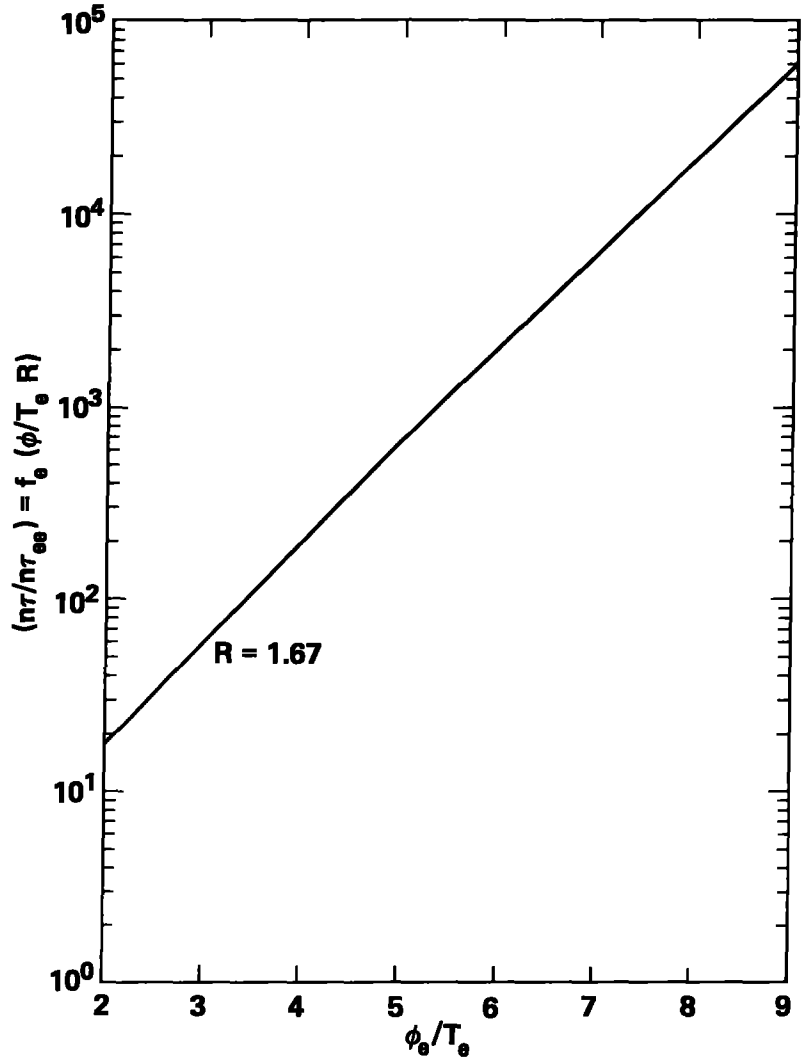

Figure B-3. For electrons we plot

$$n\tau_{pe}/n\tau_{ee} \equiv f_e(\phi_e/T_e,R) \text{ versus } \phi_e/T_e \text{ for } R = 1.67 \quad .$$

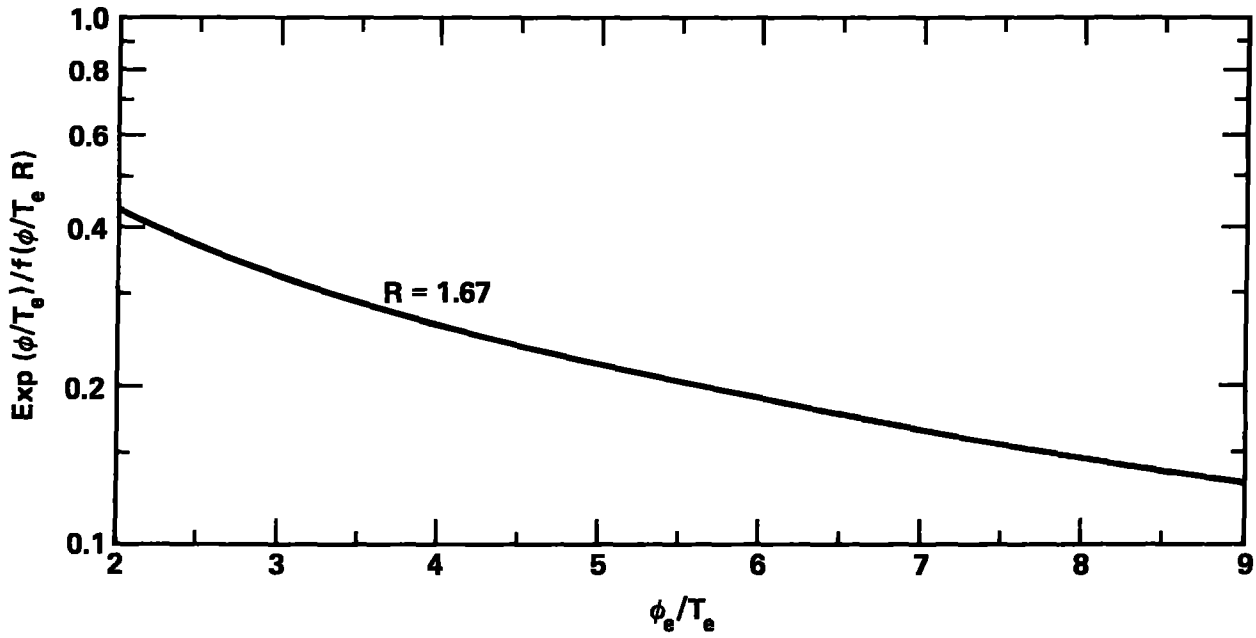

Figure B-4. For electrons we plot

$$K_e(\phi_e/T_e, 1.67) \equiv \exp(\phi_e/T_e)/f_e(\phi_e/T_e, 1.67) \quad .$$

REFERENCES

B-1. T. D. Rognlien and T. A. Cutler, "Transition from Pastukhov to Collisional Confinement in a Magnetic and Electrostatic Well," Nucl. Fusion 20, 1003 (1980).

B-2. F. Najmabadi, R. W. Conn, and R. H. Cohen, Collisional End Loss of Electrostatically Confined Particles in a Magnetic Mirror Field, University of California at Los Angeles, Los Angeles, CA, UCLA Center for Plasma Physics and Fusion Engineering Report PPG-275 (1983).

APPENDIX C: SCALING TOWARD PROPOSAL VALUES

The depth of the negative potential dip is determined by the balance between pumping and filling and is insensitive to central cell electron temperature. The necessary pumping frequency scales with the central cell density and temperature as

$$\frac{\nu_1}{\nu_0} = \frac{n_{c1}}{n_{c0}}\left(\frac{T_0}{T_1}\right)^{3/2} \quad . \tag{C1}$$

Scaling from the values of this report toward the proposal values of $n_c \simeq 10^{13}$, $T_1 \simeq 1$ keV, we find that the pumping frequency required to maintain a potential dip of $\sim$0.2 kV is

$$\nu_1 = \frac{10^{13}}{2 \times 10^{12}} \frac{0.057}{1}^{3/2} = 0.07\ \nu_0 \quad ,$$

or less than 10% of the present pumping frequency. Of course we wish to produce a barrier that is a factor of ten deeper. The condition of quasi-neutrality requires that at the barrier minimum

$$n_{eh0} = n_{trapped} + n_{pass} + n_{si} \ .$$

With increasing ϕ_B, n_{pass} decreases, while $n_{trapped}$ is unchanged (disregarding nonadiabatic trapping), and n_{eh0} and n_{si} are little affected until ϕ_B is of the order of their parallel energy. Thus, our excess pumping ability in reducing $n_{trapped}$ should be able to produce the required barrier dip.

The height of the potential peak is determined by particle and power balance. Because the central cell temperatures and the height of the potential peak will be much higher than at present, whereas the end loss currents will be about the same, the density of the untrapped electrons at the outer mirror throat should be greatly reduced. We assume for this case

$$\frac{S\hat{\tau}_p}{n_t} >> \left(\frac{T_c}{T_0}\right)^{1/2} \frac{n_m}{n_{t\ max}} \quad , \tag{C-2}$$

and solve the particle and power balance equations; we will verify the above inequality later in this report. With the above approximation, particle balance gives

$$SL = B_0 \int \frac{Sdz}{B} = \frac{B_0}{n\tau_p} \int \frac{n_t^2 dz}{B} \quad , \tag{C-3}$$

whereas power balance gives

$$(PL)_{Drag} + (PL)_{ext} = qSL \times (\phi_{EL} + T_t) \times 10^3 \ W/cm^2 \quad , \tag{C-4}$$

where ϕ_{EL}, T_t are in keV, and $(PL)_{ext}$ is an external power input.

Following the model of Sec. 3.2, but using $\langle\sigma v\rangle_{iwe} = 2 \times 10^{-8}$ to correct for higher T_t, we find

$$SL = B_0 \int \frac{sdz}{B} = 5 \times 10^3 \ n_{eh0} \quad . \tag{C-5}$$

(We have assumed that $\langle n_0 \rangle$ is unchanged.)

For $(PL)_{Drag}$, we take (assuming the density profiles of our model)

$$(PL)_{Drag}\ (he - e) = \frac{qB_0}{2.7 \times 10^5 \ E_h^{1/2}} \int \frac{n_{ew} n_{eh} dz}{B}$$

$$= \frac{q \times 4.1 \ n_{eh0}^2}{2.7 \times 10^5 \ E_h^{1/2}} = 1.5 \times 10^{-5} \ \frac{q n_{eh0}^2}{E_h^{1/2}} \ W/cm^2 \quad ,$$

and

$$(PL)_{Drag}(si - e) = \frac{qB_0 E_{si}}{10^9 \ T_t^{3/2}} \int \frac{n_{si} n_{ew}}{B} \, dz$$

$$= \frac{q \times 5.8 \ n_{eh0}^2 \times E_{si}}{10^9 \ T_t^{3/2}}$$

$$= 5.8 \times 10^{-9} \frac{qE_{si} n_{eh0}^2}{T_t^{3/2}} \text{ W/cm}^2 \quad ;$$

where the energy units are keV. Therefore,

$$PL_{Drag} = q \times \left(\frac{1.5 \times 10^{-5}}{E_h^{1/2}} + \frac{5.8 \times 10^{-9} E_{si}}{T_t^{3/2}} \right) n_{eh0}^2 \text{ W/cm}^2 \quad . \qquad \text{(C-6)}$$

Substituting Eqs. (C-5) and (C-6) in Eq. (C-4) and rearranging

$$\frac{\phi_{EL}}{T_t} = \frac{1}{T_t} \left[\left(\frac{3 \times 10^{-12}}{E_h^{1/2}} + \frac{1.2 \times 10^{-15} E_{si}}{T_t^{3/2}} \right) n_{eh0} + \frac{(PL)_{ext}}{6 \times 10^5 q n_{eh0}} \right] - 1 \; . \qquad \text{(C-7)}$$

Taking

$$n\tau_p = 4.35 \times 10^8 \, T^{3/2} \, f_e(\phi/T, R) \quad ,$$

particle balance gives for R = 2

$$T_t^{3/2} \, f_e(\phi/T, 2) = 1.75 \times 10^{-12} \, n_{eh0} \; . \qquad \text{(C-8)}$$

We consider several examples:

Central cell heating at present density--no auxiliary heating in the positive plug.

We assume enough central-cell ion heating such that n_m is reduced to where Eq. (C-2) is satisfied. Taking $n_{eh0} = 10^{12}$, $E_h = 70$, $E_{si} = 6$, $PL_{ext} = 0$, we find the solution of Eqs. (C-7) and (C-8) for $T_t = 0.143$ keV, $\phi/T_t = 2.42$, $\phi = 0.35$. If we want the central cell potential near ground with $\phi_c/T_{ic} \sim 2.5$ then T_{ic} will approximately equal 0.14 keV. Scaling the central-cell end-loss current

$$I_{EL1} = \left(\frac{n_1}{n_0} \right)^2 \times \left(\frac{T_{0ic}}{T_{ic}} \right)^{1/2} I_{EL0} \approx 0.2 \text{ A} \quad ,$$

for $n_1 = n_0$, $T_{0ic} = 0.04$ keV, $T_{ic} = 0.14$ keV, and $I_{ELO} = 1.5$ A. From this

$$n_m = \frac{2 \times 0.2}{q \times 10^6 \times 0.15 \times \pi \times (10.6)^2} (140 + 350)^{1/2} \approx 2 \times 10^9 \quad .$$

The density is close to the assumed end wall density. It follows that

$$\frac{S\hat{\tau}_p}{n_t} = \exp(-\phi/T_t) = 0.09 >> \left(\frac{0.143}{0.005}\right)^{1/2} \left(\frac{2 \times 10^9}{4 \times 10^{11}}\right) = 0.03 \quad ,$$

so the condition of Eq. (C-2) is satisfied.

We conclude that a moderate amount of isotropic central-cell ion heating applied to the type of plasma presently obtained should result in an end-loss-potential increase by a factor of three.

Central cell heating at proposal density--no auxiliary heating in the positive plug.

We scale the density times 5 to calculate values close to the proposal values. We assume that the background neutral density fueling the positive peak is unchanged. We also assume heating of the central-cell isotropic-ion component. Taking $n_{ehO} = 5 \times 10^{12}$, $E_{si} = 6$ keV and $E_h = 38$ keV (to keep the plug $\beta \approx 0.3$) we find solution of Eqs. (C-7) and (C-8) for $T_t \simeq 1$ keV, $\phi/T_t = 1.47$, and $\phi \simeq 1.47$ kV. For the central cell potential near ground with $\phi_c/T_{ic} \simeq 2.5$, we need $T_{ic} \approx 0.6$ keV.

Central cell heating at proposal density--auxiliary heating in the positive plug.

We assume the same values as above, $n_{ehO} = 5 \times 10^{12}$, $E_{Si} = 6$ keV, and $E_h = 38$ keV; and solve Eqs. (C-7) and (C-8) for several values of $(PL)_{ext}$, the auxiliary heating power per cm^2. We also assume that the power is isotropic. These results are plotted in Fig. C-1. Very little improvement is gained by the auxiliary isotropic heating because the potential is limited by the cold-electron feed rate.

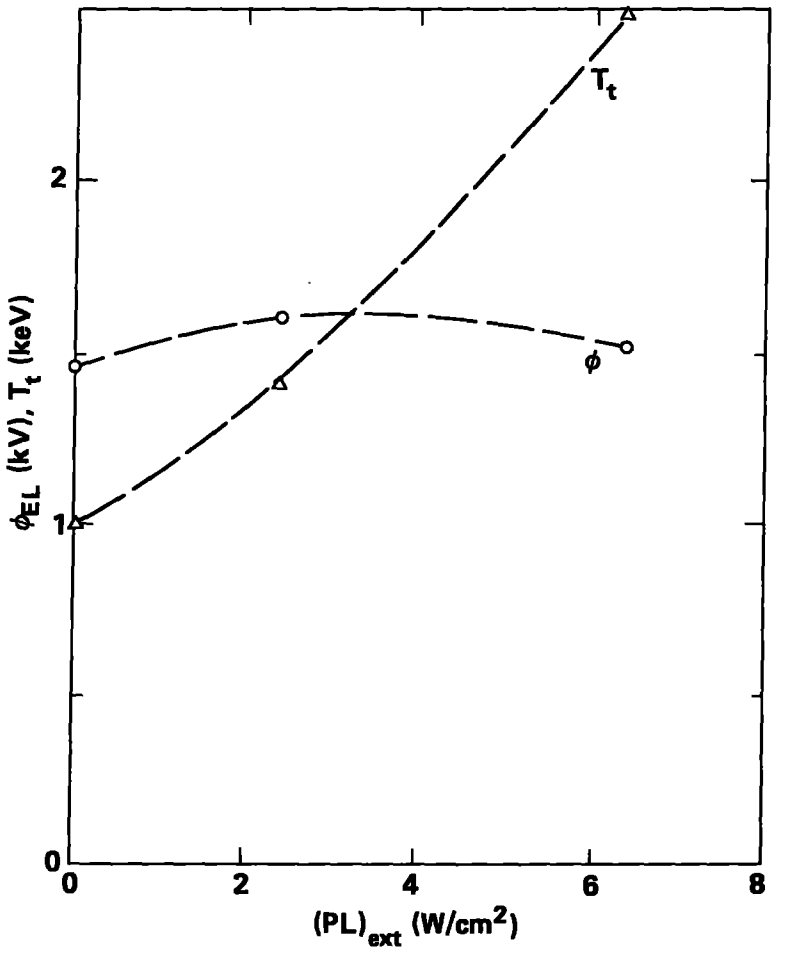

Figure C-1. Positive potential plug parameter vs auxiliary heating power.

The obvious attack on this problem is to reduce the cold-electron feed rate by reducing the neutral density and/or by better shielding of the fans. Improvement can also be made by dropping out neutral beams because our experiment shows that $I_b \tau_{ex} \approx$ constant, but this is at the expense of barrier pumping. Strong rf heating may also be used, but this may upset the stability of the balanced mode. Further modeling is needed.

4643v/EP/RP/MM